PAPER

www.rsc.org/loc

Combinatorial mixing of microfluidic streams†

Christopher Neils,[a] Zachary Tyree,[b] Bruce Finlayson[b] and Albert Folch*[a]

[a] *Department of Bioengineering, University of Washington, Seattle, Washington 98195-2255, USA. E-mail: afolch@u.washington.edu; Fax: 1 206 543 6124; Tel: 1 206 685 2257*

[b] *Department of Chemical Engineering, University of Washington, Seattle, Washington 98195-1750, USA. E-mail: finlayson@cheme.washington.edu; Fax: 1 206 685 3451; Tel: 1 206 685 1634*

Received 19th November 2003, Accepted 22nd March 2004
First published as an Advance Article on the web 23rd April 2004

We have devised a microfluidic mixer design that produces all the mixture combinations of a given number of dilutions of the input compounds. As proof of the concept, we present a device that generates four titrations of two dye solutions, blue and yellow, and combinatorially mixes the blue titrations with the yellow titrations to deliver the sixteen mixture combinations in separate outlet microchannels. Our device features four different flow levels made by stacking nine laser-cut Mylar laminates. The fluidic network has a symmetric design that guarantees that the flow rates are the same at all the outlets, with deviations attributable to imperfections in the fabrication, assembly, or perfusion processes. Design rules for scaling up the number of compounds and/or dilutions are presented. The mixing scheme has broad applicability in high-throughput combinatorial testing applications such as drug screening, cell-based biochemical assays, lab-on-a-chip devices, and biosensors.

Introduction

Living systems are sustained by complex, highly coupled biochemical reactions;[1,2] hence, their response to manipulation with multiple chemical or biochemical compounds often can not be extrapolated from tests with single compounds. Therefore, tests of potentially coupled and non-linear responses (*e.g.*, in drug testing or biological assays) typically include multiple combinations of multiple dilutions. As our understanding of living systems expands, so does the number of combinations to be tested, and conventional large-scale testing approaches based on robotic fluid handling and multi-well plates become increasingly expensive, impractical, or infeasible.

Microfluidic tools have addressed some of the challenges associated with present analytical approaches, by performing analyses more rapidly and with less reagent consumption. Miniaturized equipment for capillary electrophoresis[3–5] and chromatography[6–8] have been used to analyze DNA,[9] proteins,[10–13] and pharmaceutical compounds.[14,15] Microfluidic devices have also found applications in cell sorting,[16,17] delivery of chemical compounds to cells,[18,19] and protein crystallization.[20,21] Although microfabricated systems can perform biochemical tests rapidly, they often face a bottleneck when testing different concentration levels of several compounds: most devices still require that the mixtures of dilutions be produced outside the device using macroscopic tools (*i.e.* a robotic dispenser or a human-operated pipette) prior to introduction into the microfluidic device. Given the time involved in manually mixing and dispensing solutions and the cost of robotic equipment and biochemical reagents, there is a strong need for combinatorial mixers capable of creating all the desired combinations of mixtures from small amounts of the input solutions.

Experimental

Fabrication

Our combinatorial mixing device was created by laminating 100 μm thick sheets of high-transparency polyethylene terephthalate (Mylar® D, Dupont)[22] to make a three-dimensional microfluidic network. Channel and window patterns were cut using a CO_2 laser engraver (Model M20, Universal Laser Systems, Scottsdale, AZ). Every other layer of Mylar carries, on both sides, a dry adhesive coating ~25 μm thick (501FL, 3M) and backing sheets that are also cut by the laser (Mylar + adhesive from Fralock, Canoga Park, CA). The laser cutter is computer controlled through vector drawing software and a Windows®-based printer driver (see Table S-1 in Electronic supplementary information (ESI) † for our cutting parameters). The cut Mylar laminates are aligned, bonded and pressed to create a multilayer structure that contains a microfluidic network.

Operation

The Mylar device was connected to external tubing *via* a molded silicone rubber connector. The connector block included four holes; each hole was 3.2 mm diameter at one end (to accept external tubing) and 1.6 mm at the other end (to fit over inlet holes in the top Mylar layer). The device was immersed and filled with filtered (0.2 μm pore size), degassed water before dyes were introduced. One percent solutions of FD&C Blue #1 and Yellow #6 (Spectrum Chemicals, *via* Cole Parmer, Vernon Hills, IL) in water, and water as diluent, were driven by computer-controlled twist-drive syringe pumps (microFlow System, Micronics Inc., Redmond, WA).

Imaging

Microscopic images were captured using a Nikon CoolPix 990 digital camera mounted on a Nikon SMZ-1500 stereomicroscope.

Results and discussion

In small channels, the flow of liquids at low to moderate velocities is laminar (*i.e.* free from convective eddies) because the momentum of the liquid is negligible compared to viscous drag forces. This ratio of momentum to viscous forces is expressed by the Reynolds

† Electronic supplementary information (ESI) available: Details on the numerical model of serpentine channel, uniformity analysis, ratiometric analysis, and derivation of geometric mean as stream boundary; laser cutting parameters; colorimetric analysis; volumetric flow rates from the finite difference model, color density measurements after junctions in the joining array, and the CorelDraw® file of window patterns for the laser cutter. See http://www.rsc.org/suppdata/lc/b3/b314962e/

DOI: 10.1039/b314962e

number, $Re = ud/\nu$, where u is the average flow velocity, d is a length dimension, and ν is the kinematic viscosity. Typically flow is laminar when $Re < 2000$ and d is a transverse channel dimension (here, the channel depth).[23,24] We operated the device reported here with Re in the range $0.01 \leq Re \leq 2$. Reported strategies to enhance mixing include (a) dividing and recombining the flow streams,[25–28] (b) passing flow through a 3D "serpentine" channel,[29–31] (c) using oblique ridges[32] or arrays of micronozzles[33] to force transverse flow, and/or (d) electrokinetic means.[34,35] Our device contains 51 serpentine mixers.

Previously, several groups have reported designs that generate microfluidic dilutions. Dertinger *et al.*[36] demonstrated a symmetric two-dimensional (2D) microfluidic network that continuously generates certain combinations of dilutions of two compounds; the output concentrations can be straightforwardly predicted by symmetry considerations, but not all the combinations are possible. For example, in one configuration a device with two inlets can create a series of mixtures with increasing dilutions of A and decreasing dilutions of B, but a separate configuration would be needed to produce a series with increasing dilutions of both A and B. Independent mixing and dilution clearly require three-dimensional (3D) networks[37,38] that allow channels to pass over one another. Ismagilov *et al.*[39,40] have demonstrated orthogonal channel arrays that create a potential mixing point at every channel intersection; methods to control mixing have included channels with variable aspect ratio[39] and microporous membranes.[40,41] Another 3D device converted four inlets into four undiluted binary mixtures.[42] However, none of these devices allowed for combinatorial mixing of all the dilutions of the input compounds. Microfluidic systems that dilute and/or mix solutions in batches using valves and stopped flow[43,44] can sequentially produce any desired dilution mixture(s), but they do not provide a continuous outlet stream (*e.g.*, for a constant cell culture environment).

Here we report the design and successful operation of a microfluidic combinatorial mixer that (1) accepts two test solutions and two diluting streams, (2) internally generates four dilutions of each solution, and (3) combinatorially mixes the dilutions, producing 16 output streams, each carrying a different mixture combination. Importantly, the combinatorial device is symmetrically designed such that (a) all the output flow rates are equal (to the precision permitted by the microfabrication technique), and (b) the number of compounds and/or dilutions per compound can be scaled up without significant reanalysis.

Nomenclature and conceptual design

Fig. 1 presents a modular schematic diagram of the combinatorial mixer. Each "4× distributor" splits one input stream into four outputs, and each "4× diluter" generates four dilutions from two inputs. Distributors use binary and symmetric branches to distribute flow equally (in the absence of fabrication inaccuracies and differences in downstream flow resistance).

Our prototype creates 16 combinatorial mixtures of two dyes from four inlets – one for each dye (here, yellow and blue) and two for water. On the left side of the network shown in Fig. 1, yellow dye and water first enter a diluter, producing four dilutions that are labeled Y_0 (pure water), Y_1, Y_2, and Y_3 (undiluted yellow). Next, a row of 4× distributors splits each yellow dilution channel into four separate channels. The result is 16 channels with the following concentration sequence:

Y_3, Y_3, Y_3, Y_3, Y_2, Y_2, Y_2, Y_2, Y_1, Y_1, Y_1, Y_1, Y_0, Y_0, Y_0, Y_0.

On the right side of the device, blue dye and water first enter a 4× distributor with bridges that produces four pairs of channels in the sequence B_3, B_0, B_3, B_0, B_3, B_0, B_3, B_0. Each pair enters a separate diluter to generate four dilutions of blue; these solutions are labeled B_0 (pure water), B_1, B_2, and B_3 (undiluted blue). The result is 16 streams in the following blue concentration sequence:

B_3, B_2, B_1, B_0, B_3, B_2, B_1, B_0, B_3, B_2, B_1, B_0, B_3, B_2, B_1, B_0.

The Y_0, Y_3, B_0, and B_3 solutions remain unchanged from the inlets, and the intermediate concentration values of Y_1, Y_2, B_1 and B_2 are dictated by the physical design and performance of the device. It is important to note that a distributor that feeds into a row of diluters (here, the blue distributor) must split and bridge microchannels over each other in order to achieve the output sequence, whereas distributors that come after a diluter do not need to bridge microchannels.

The 16 blue channels meet the 16 yellow channels in a linear array of fluid junctions, labeled "joining array" in Fig. 1. The first channel in the yellow sequence meets the first channel in the blue sequence, the second yellow channel meets the second blue channel, and so on, to produce all 16 combinations of one yellow dilution (Y_3, Y_2, Y_1 or Y_0) with one blue dilution (B_3, B_2, B_1 or B_0): $Y_3 + B_3$, $Y_3 + B_2$, $Y_3 + B_1$, $Y_3 + B_0$, $Y_2 + B_3$, $Y_2 + B_2$, $Y_2 + B_1$, $Y_2 + B_0$, $Y_1 + B_3$, $Y_1 + B_2$, $Y_1 + B_1$, $Y_1 + B_0$, $Y_0 + B_3$, $Y_0 + B_2$, $Y_0 + B_1$, and $Y_0 + B_0$. We note that equal mixing of two streams, each with one dye, necessarily dilutes the concentration of each dye by 50%, so the initial dye concentrations must be selected accordingly.

3D microfluidic network

Our proof-of-concept combinatorial mixer incorporates the dilution, distribution, and joining functions in a 3D microfluidic network occupying four flow levels. The flow levels are separated by additional Mylar layers that contain windows to connect the flow channels, for a total of nine layers. Perspective drawings of the 3D structure of selected parts of the microfluidic network are shown in Fig. 2, beside corresponding images of the operating device (Fig. 2A–C and E).

There are no valves or pumps in the microfluidic device, so mixing ratios are governed only by the static flow network and the

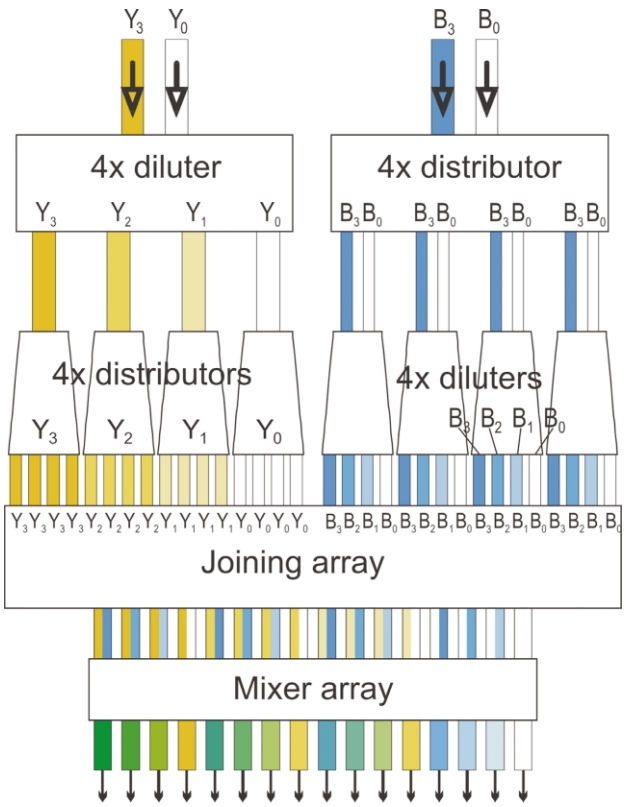

Fig. 1 Conceptual diagram of the 4 × 4 combinatorial mixer. The yellow dye (Y_3) and diluent (Y_0) pass first through a diluter and then through a row of distributors, creating 16 yellow streams containing 4 titrations. The blue dye (B_3) and diluent (B_0) pass through a distributor first, then through a row of diluters that repeat the same titration sequence four times. The joining array overlays the yellow dye series atop the blue dye series and combines each pair of yellow and blue streams into one channel.

(controllable) flow rate into each inlet. Each half of the device is laid out in a design that provides equal flow resistance, and hence flow rate, along the 16 flow paths from an inlet to the joining array. Flow paths in the yellow half of the device do not need to match the paths in the blue half and the flow balance does not require the two halves to be equidistant from the joining array. In fact, a drop of water travels ~118 mm along each flow path in the yellow side, and ~103 mm through each blue path. Flows can be balanced in spite of differences in path length by controlling the inlet flows with a volumetric source (*e.g.*, syringe pumps) or by adjusting a pressure source (*e.g.*, gravity) appropriately.

Mixer fabrication

Our microfluidic network was assembled by stacking and gluing laser-cut sheets of high-grade Mylar, a transparent polyethylene film. Laser cutting and assembly took about 3 h for our nine-layer prototype. The precision of our fabrication technique is determined primarily by the resolution of the laser cuts and the precision of alignment when assembling the stack. As configured, our CO_2 laser system has a nominal positioning accuracy of 25 μm and laser spot size of about 150 μm. A single full penetration cut in 100 μm thick Mylar leaves a gap that is approximately 250 μm wide. Long channels cut in the same sheet must be spaced at least 500 μm apart to ensure adhesion of the intervening strip of Mylar, but 3D layering allows the microchannels to be packed more densely. For example, serpentine mixers in the outlet array occupy the width of two channels and would intersect if the mixers were coplanar. Alternating the vertical position of the mixers allows the mixers to be placed with the same spatial frequency as the straight channels. We note that assembling a device in which the entire blue network is directly over the yellow network would have required only one additional cutting and alignment step and would have nearly halved the area occupied by the current device. However, very compact designs with many overlapping flows can be confusing to visualize and analyze, thereby complicating device optimization.

The flow through any channel network is determined primarily by the channel features that have the highest flow resistance. To

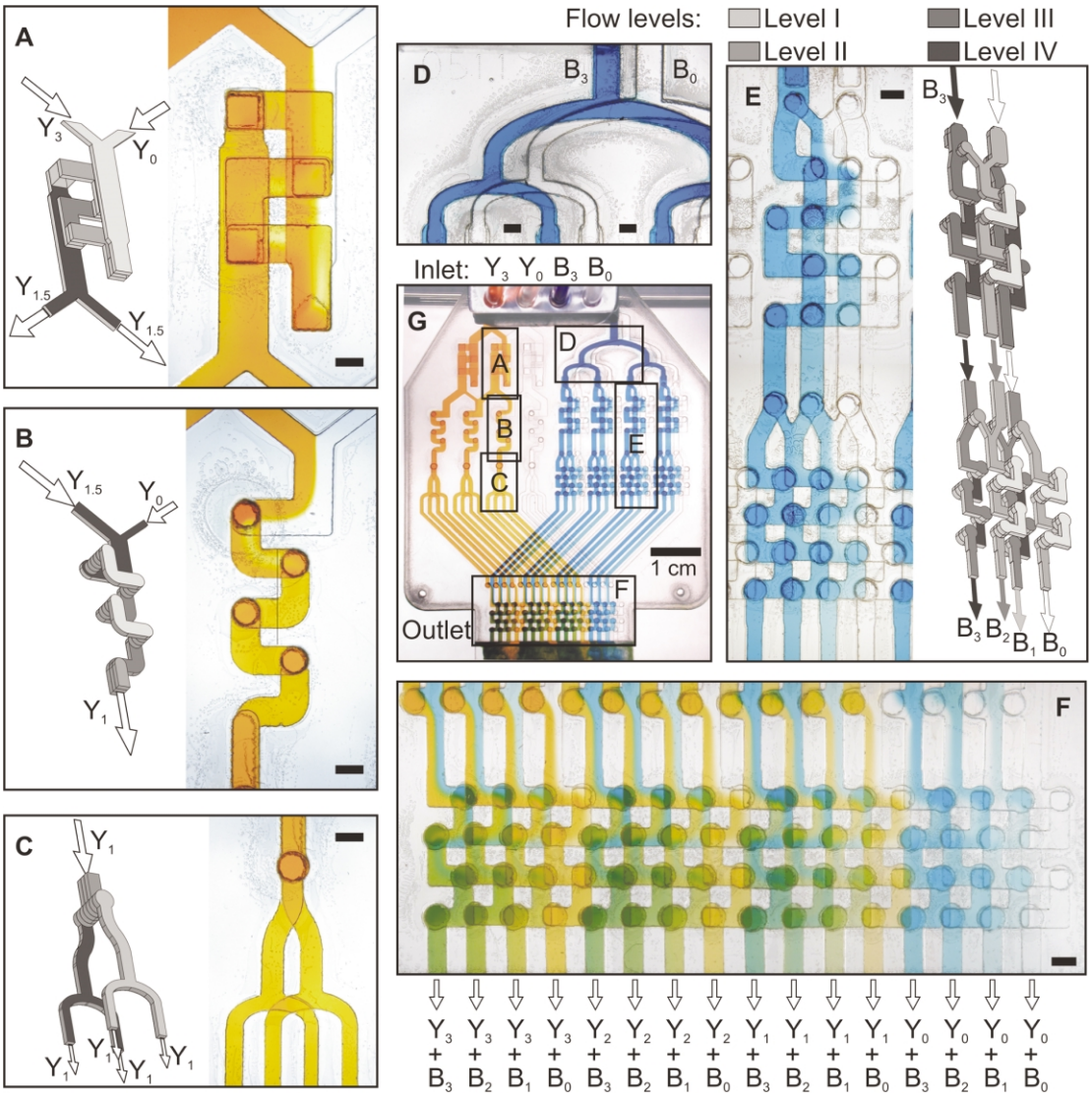

Fig. 2 Details of the combinatorial mixer, from locations shown in the central image. Flow is from top to bottom, as indicated by arrows. In the perspective drawings (A, B, C, D, E), different shades of gray correspond to the different flow levels (I–IV) where the channels reside. The subscripts on Y (yellow) and B (blue) indicate the proportional dilution, where Y_3 and B_3 are full dye concentration and Y_0 and B_0 are pure water. (A) The $Y_{1.5}$ solution is a 1:1 mixture of the Y_3 and Y_0 solutions, which are mixed in large serpentine mixers that double back to increase the fluid contact time. (B) The Y_1 solution is mixed in a smaller serpentine mixer (the Y_2 solution, not shown, is similar). (C) After mixing, each stream is divided among four channels in two splits; only the Y_1 solution is shown here. The first split is vertical in order to place the flows in the top and bottom flow levels. (D) The blue sequence starts by dividing each inlet stream four ways in a binary arbor featuring 300 μm deep channels. (E) Dilution is performed by four identical diluters. Each serpentine mixer occupies only two levels (I–II or III–IV), allowing them to overlap in order to save space. (F) Yellow dye arrives at the joining array in levels I and IV, meeting the blue dye in levels II and III. The joined streams pass through another row of serpentine mixers before leaving the device as homogeneous combinatorial mixtures. Flow through each device inlet is approximately 0.1 μL s^{-1}. Scale bars are 1 mm.

avoid flow imbalance, each window between flow levels must remain larger than the cross-section of the adjoining channels, after layer misalignment and the presence of beading at the laser cut edges are taken into account. In our experience, the factor that contributes most to variability in the flow resistance is the size of the bead ($\sim$25 μm) that forms along the laser cut edge of the Mylar. The lateral alignment of windows between flow levels also contributes, but is less important because the flow area through the windows is much greater than the flow area through the adjoining channels. The tolerance imposed by the Mylar lamination technique depends on the lateral distance that cut lines are offset to prevent the beads in adjacent layers from coinciding; in our case, we sought alignment to within 200 μm. We note that the similarity between parallel channels is more important than the exact dimensions of a particular channel design (because the mixing ratios are determined by a flow balance), and that small, random fluctuations in the channel width are not important because their net effect is minimal when averaged over the length of the channels. Although minor variations in the channel height ($\sim$100 μm) can affect the flow balance, we have found the thickness of the Mylar to be quite consistent.

Combinatorial mixer operation

Fig. 2 shows our proof-of-concept combinatorial mixer as it generates 16 combinations of four dilutions of two dyes. The flow rate is nominally 6.0 μL min^{-1} at each inlet, corresponding to an average flow velocity near 300 μm s^{-1} through the outlet channels. We note that the color density depends on the dye concentration as well as the channel depth, which can be 100 μm, 300 μm, or 500 μm (depending on whether the fluid spans 1, 3, or 5 Mylar layers, respectively).

The left side of the device (Fig. 2A–C) produces four concentrations (Y_3, Y_2, Y_1, and Y_0) from inlet streams that supply yellow dye (Y_3) and water (Y_0). Dilution is achieved with a two-stage diluter adapted from Dertinger *et al.*[36] The first stage diverts and mixes half of each inlet stream, producing three channels that contain Y_3, combined $Y_3 + Y_0$ (which we term $Y_{1.5}$), and Y_0. The second stage comprises four channels and operates on the same principle as the first stage: from left to right, the second-stage channels receive Y_3 only, one part Y_3 and two parts $Y_{1.5}$, two parts $Y_{1.5}$ and one part Y_0 (shown in Fig. 2B), and Y_0 only. The four resulting streams are Y_3, Y_2, Y_1, and Y_0, where the exact concentrations of Y_2 and Y_1 depend on the precision of fabrication and/or the pumping rates. As long as the network is balanced and the mixtures are homogenized (which does not hold true at arbitrarily high flow rates), then $Y_1 = 1/3 \times Y_3$, $Y_{1.5} = 1/2 \times Y_3$, and $Y_2 = 2/3 \times Y_3$. A detailed analysis of these measurements is presented later.

Each channel includes a 3D serpentine mixer to speed mixing after the branches meet. The serpentine channels in the first stage of the yellow diluter (Fig. 2A) double back to increase the channel length without increasing the overall length of the device. Serpentine channels in the second stage of the diluter are not as wide and do not double back (Fig. 2B). In both cases, the confluent streams are distinct just downstream of each combining junction, and have a uniform appearance by the end of the mixing channel. Quantitative analyses of the mixers' effectiveness and of the operating device are presented later and confirm the effectiveness of the complete design.

Because the diluter design relies on symmetry to balance flows, the Y_3 and Y_0 channels include serpentine mixers even though these streams are already homogeneous. In addition, parallel channels that carry different flow rates (*e.g.*, the Y_3 to $Y_{1.5}$ branch *versus* the Y_3 to Y_3 branch) have been sized to provide approximately equal flow velocity (and hence pressure drop) in each channel.

After the diluter, the four channels carrying concentrations Y_3, Y_2, Y_1 and Y_0 are split into sixteen channels by a row of 4× distributors (Fig. 2C). To save space in each 4× distributor, the first 2× subunit branches out of the primary plane of flow, into the upper and lower levels. The second rows of 2× distributors are on two different fluidic levels, allowing the resulting channels to be effectively placed closer than the laser cutting technique would allow if all the channels were coplanar. (Although the branches in the second 2× distributor are bridged to save space, the bridges do not affect the output sequence and, thus, this distributor is in essence a 2× distributor without bridges.) In sum, after the diluter and the distributors, the four yellow dilutions are organized in 16 microchannels as follows (from left to right in Fig. 2G):

Y_3, Y_3, Y_3, Y_3, Y_2, Y_2, Y_2, Y_2, Y_1, Y_1, Y_1, Y_1, Y_0, Y_0, Y_0, Y_0.

We next analyze the production of blue dilutions in the right side of the device. First, the B_3 and B_0 inlet streams are split four ways using 300 μm deep symmetric binary arbors in different flow levels (Fig. 2D). The arbors are bridged to produce four pairs of B_3 and B_0 containing channels. Each pair feeds a two-stage diluter (Fig. 2E) that is schematically equivalent to the yellow diluter, *i.e.* the first stage produces B_3, $B_{1.5}$, and B_0, and the second stage produces B_3, B_2, B_1, and B_0. The serpentine mixers in the blue diluters include two complete coils, similar to the second stage mixers in the yellow diluter. After the distributor and the diluters, the four blue dilutions are organized in 16 microchannels as follows (from left to right in Fig. 2G):

B_3, B_2, B_1, B_0, B_3, B_2, B_1, B_0, B_3, B_2, B_1, B_0, B_3, B_2, B_1, B_0.

The 16 yellow channels and the 16 blue channels turn diagonally to meet in the joining array (Fig. 2F), which merges the concentration sequences so each pair of yellow and blue dilutions enters one microchannel. The blue and yellow fractions stay visible until the joined streams pass into a final row of serpentine mixers, after which the combinatorial mixtures are visible as multiple shades of green, blue, yellow and clear.

Data analysis

We have calculated the composition of each solution at the device outlets using two steps: (a) a uniformity analysis to confirm the thoroughness of mixing in the serpentine mixers, and (b) a ratiometric analysis to determine the relative contributions of the Y_3 and Y_0 (or B_3 and B_0) inlet solutions in the outlet channels. For comparison, a colorimetric analysis of the dilution sequences is presented in Fig. 3 (see ESI† for details). The colorimetric measurements are subject to spatial and gray scale non-linearity in the imaging system, as well as refraction in the glue layers, so these results provide only qualitative support of the ratiometric analysis. A photometric analysis with fluorescent dyes would provide a more direct relationship between signal strength and dye concentration, but was not undertaken here due to the autofluorescence of Mylar.

Uniformity analysis

Our ratiometric prediction of dye dilution shown below assumes that the dye solutions are uniform wherever branching occurs. Therefore, we begin by analyzing the performance of the serpentine mixers, which we have numbered by size using Roman numerals, from I (smallest) to IV (largest). Their relative sizes are shown in Fig. 4.

In order to understand the performance of the serpentine mixers better, we have developed a finite-element model of flow through a small (size I) serpentine channel (see ESI† for details). Fig. 5 shows a thermal color plot of the concentration distribution predicted along the channel walls and at selected cross-sections when the flow rate is 0.1 μL s^{-1} and the diffusion coefficient of the dye is 4.5×10^{-10} m^2 s^{-1}.[45] The figure illustrates how the combined vertical and lateral turns expand the diffusion interface. For example, the dark blue edge of the channel becomes light blue immediately after the first vertical turn because a portion of the opposing (red) stream has been folded underneath.

Fig. 6A shows a size I mixer with the same flow rate as in Fig. 5 (0.1 μL s^{-1}, Re = 0.125). Plots accompanying the micrograph illustrate the following quantitative analysis, in which the effectiveness of each size of serpentine mixer was measured as a function of flow rate (see 'Uniformity analysis' in ESI† for procedural details). The mixers were evaluated experimentally by observing how visible concentration gradients diminish as two distinct solutions — one with dye and one without — flow through the channel.[46] Dedicated test devices were made to obtain unobstructed images of mixer sizes I to III, and the 4 × 4 combinatorial device itself was used to test the size IV mixer. The mixing progress was derived from gray scale images by plotting the pixel values along imaginary lines perpendicular to the serpentine channel. We have expressed the progress of mixing at any given point along a serpentine channel as the ratio of the gray level range at that point (G) to the gray level range at the inlet (G_{in}). This "unmixed ratio" ($R = G/G_{in}$) approaches zero as the gray scale profile becomes more uniform. Near the inlet, plots of the 100% and 0% dye regions are flat and distinct (R = 1), after one turn a monotonic gradient reaches nearly all the way across the channel (R = 0.60), and after all four turns the concentration profile is flat to within 13% of the initial gray scale range (R = 0.13).

The flow rate has a significant effect on the homogeneity of the mixture exiting from a serpentine mixer. As an example, Fig. 6 shows the size I mixer during operation at three flow rates. When the flow rate was 0.01 μL s^{-1}, diffusion was apparent before the stream enters the first lateral turn (Fig. 6B). When the flow rate was 0.075 μL s^{-1} (Fig. 6C), the boundary was distinct into the first change of level and gradients were visible through the second change of level. Flow at 0.4 μL s^{-1} (Fig. 6D) produced a sharp boundary even after the first turn, and gradients were still visible in the outlet channel. We note that the region of highest dye concentration started in the left left-hand side of the channel, moved to the right-hand side after two level changes, and ended up in the center of the channel.

Fig. 7 compares the unmixed ratio $R_{out} = G_{out}/G_{in}$ at the outlet of all mixer sizes at selected flow rates ranging from 0.01 to 0.8 μL s^{-1} per channel. The performance of the three smaller mixers is similar, which can be understood from a theoretical consideration of the Peclet number (Pe) of the flow in the straight sections within the serpentine mixers. Here we use the definition $Pe = uW/D$,

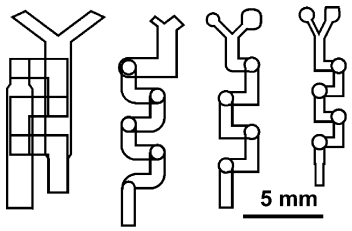

Fig. 4 Relative sizes of the four serpentine mixers. The mixers are ordered by size, from the largest (size IV) on the left, to the smallest (size I) on the right. The outlines are taken from the computer drawing file, and each laser-cut channel is approximately 200 μm wider than shown.

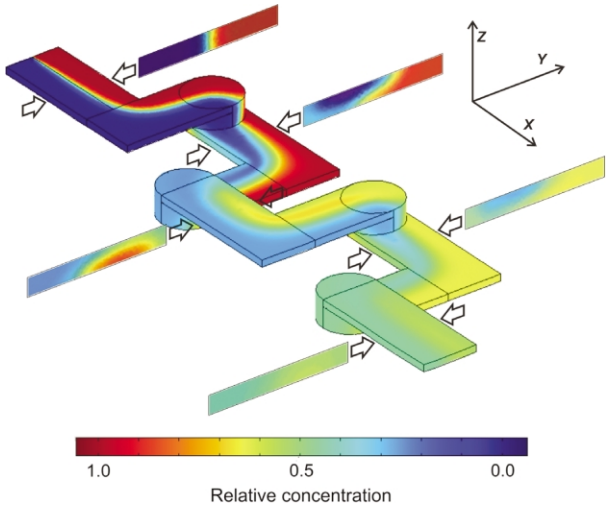

Fig. 5 Finite-element model of mass transfer in a size I mixer. The "serpentine" geometry of the channel enhances mixing by twisting the diffusion interface. Colors indicate the local concentration of red 'dye' as a fraction of the inlet conditions. The main figure shows the concentration at the channel walls, and the inset images show cross-sections in the y-z plane. The width and height of the flat channel are 800 μm (dimensionless value of 1) and 100 μm (dimensionless value of 1/8), respectively; the Reynolds number equals 0.125 (flow rate = 0.1 μL s^{-1}) and the Peclet number equals 2220 ($D = 4.5\times10^{-10}$ m^2 s^{-1}).

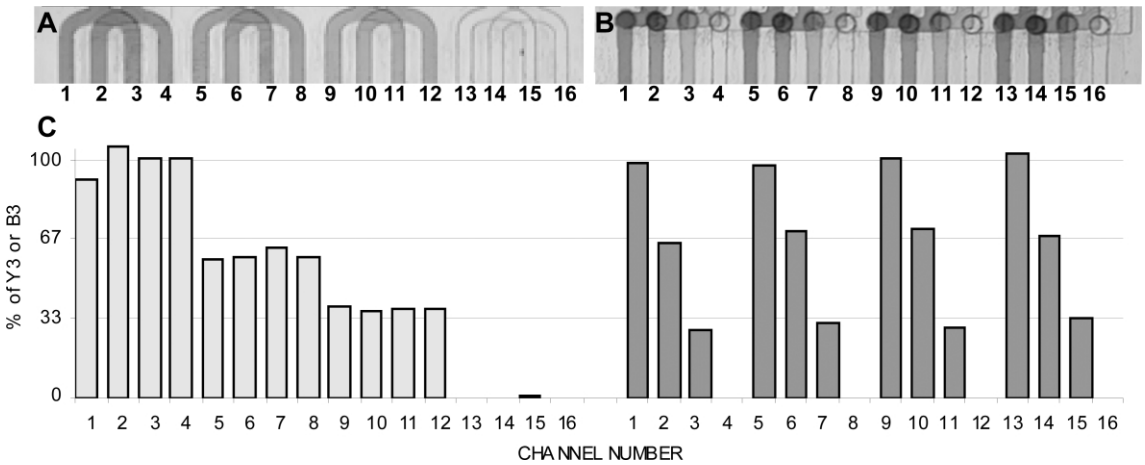

Fig. 3 Results of colorimetric analysis of the concentration sequences. Pixel values were extracted from gray scale images of the four 4× distributors downstream of the yellow diluter (A), and of the exits from the four small blue diluters (B). The gray levels were converted to concentration values (C) as follows: (1) the average gray level of pixels in a rectangular region of each channel was recorded; values were subtracted such that the zero gray level was the average from the four Y_0 (or B_0) channels; (2) the gray scale data were converted into light transmittance values, using an exponential curve fit to account for the finite absorption by the Y_3 dye; (3) finally, the transmittance values were converted to a concentration (fraction of Y_3) by taking the multiplicative inverse of the logarithm, consistent with Beer's Law. The yellow dye results are plotted by treating the average gray level in the Y_0 channels (numbers 13–16) as zero and the average gray level in the Y_3 channels (numbers 1–4) as 100. The blue dye concentrations are plotted using the B_0 channels (numbers 4, 8, 12, and 16) for zero and the B_3 channels (numbers 1, 5, 9, and 13) for 100. This method is approximate because the conversion includes an estimation of the gray level associated with infinite dye concentration, but given the approximations above the results strongly support the conclusions of the ratiometric analysis (see main text).

where u is the average fluid velocity, W is the channel width and D is the diffusion coefficient of the dye in water. Thus, Pe is an indicator of the extent of lateral diffusion per unit length of flow.[47] The average fluid velocity u may be written as q/hW, where q is the volumetric flow rate and hW is the flow area in the channel (*i.e.* the product of channel depth and width). The Peclet number may then be expressed as q/hD, so graphing as a function of flow rate is equivalent to graphing as a function of Pe. The values for Pe are shown along the top of Fig. 7, and range from 220 to 17000. The three smaller mixers have a similar shape (*i.e.* length, number and direction of turns) so we would expect the same extent of lateral diffusion at any given flow rate (and, hence, Peclet number).

The largest (size IV) mixer produced less homogeneous mixtures at the tested flow rates than the small (sizes I to III) mixers did. We attribute this result to the following two reasons: (a) The size IV mixers have one less perpendicular out-of-plane turn than the smaller mixers, in order to double back and increase channel length; and (b) the channels in the size IV mixers — which were sized in proportion to the flow that passes through them — were so wide that the vertical turns were not sufficiently out of the flow plane to be effective. As with any serpentine mixer, the performance of the size IV mixers at high flow rates could be improved by adding another out-of-plane turn, by reducing the channel width, and/or by increasing the channel depth from 100 μm to 300 μm in some locations (thereby slowing the flow and expanding the interface between solutions). As an alternative, mixing in the first stage of the diluter could be improved by substituting the size III mixers for the size IV mixers.

As the flow rate increases, the compounds have less time to diffuse and the serpentine mixers become less effective. Nevertheless, the mixtures may still be considered combinatorial because all of the combinations of Y_m and B_n are produced, even though Y_m and B_n do not represent evenly spaced dilutions. For applications where non-linear responses are to be expected, uneven spacing may even be preferable to linear spacing. Fig. 4E suggests that predicting the output concentrations at flow rates greater than ~0.1 μL s^{-1} per mixing channel would require computational fluid dynamics methods.

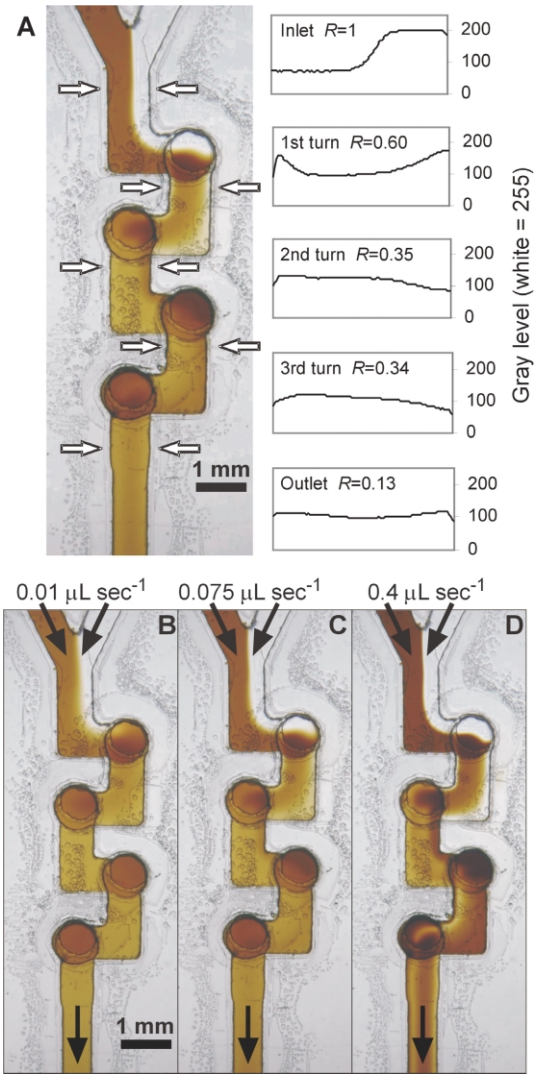

Fig. 6 (A) Optical micrograph of mixing in a size I serpentine mixer with 0.1 μL s^{-1} flow. Plots show the gray levels along lines that connect each pair of white arrows. Mixing is quantified by comparing the total range of gray values present in each plot (G) to the range present in the inlet plot (G_{in}). The ratio of these ranges, $R = G/G_{in}$, is shown for each plot. (B–D) Optical micrographs of flow through a size I serpentine mixer. Flow rates indicate the sum of the two inlet streams. At 0.01 μL s^{-1}, diffusion is apparent before the beginning of the mixer; at 0.075 μL s^{-1}, the solution needs only two turns to mix; at 0.4 μL s^{-1}, stripes remain visible in the outlet channel.

Ratiometric analysis

If the flow rates at all the device inlets are equal and the solution exiting each serpentine mixer is well mixed, then the dye concentrations downstream of each diluter can be determined indirectly from the contribution of each stream at every confluent junction.[36] Obviously, the composition is known in every Y_3, Y_0, B_3 and B_0 channel because each one contains only pure dye or water. For the remaining channels, the flow ratio can be determined from images of the operating diluters. First, a profile of the dye concentration across each channel is generated from a gray scale image taken downstream of each combining junction. The interface between the flow streams is then defined as the location where the dye concentration is the arithmetic mean of the concentrations in the two incoming streams. According to Beer's Law, the light transmittance through a flat channel of height h is a negative exponential function of the dye concentration C and its extinction coefficient ε.[48]

$$I_{out}/I_{in} = e^{-hC\varepsilon} \quad (1)$$

From this relationship it can be shown that the arithmetic mean of two concentrations corresponds to the geometric mean of their transmittances; hence, the interface location is located where the profile plot equals the geometric mean of the high and low gray values observed in the channel (see 'Ratiometric analysis' in ESI† for derivation).

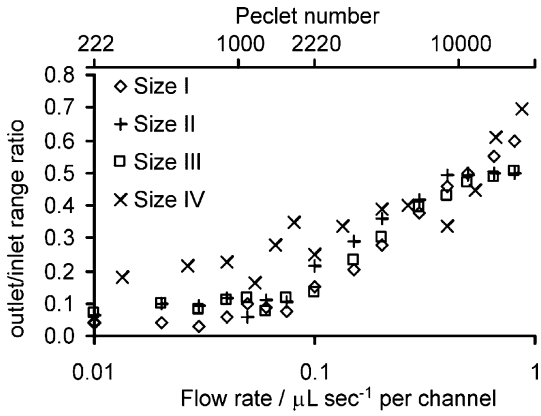

Fig. 7 Plot of the unmixed ratio at the outlet R_{out} as a function of flow rate and Peclet number (logarithmic scales), comparing all four serpentine mixer sizes. Here, $R_{out} = G_{out}/G_{in}$ (outlet gray scale range G_{out} divided by the inlet gray scale range G_{in}). A value of $R_{out} = 1$ indicates that the solution is not thoroughly mixed (the condition at the inlet), while $R_{out} = 0$ when the dye concentration is uniform. The Peclet number is proportional to flow rate with a proportionality constant of $1/hD$, where hD is the product of channel height and mass diffusion coefficient. The total path length between the measurement locations is 11.8, 15.4, 17.2 and 30.5 mm for mixer sizes I through IV, respectively.

The interface location can be converted into a flow fraction by accounting for the low flow velocity near the channel walls. Due to this low velocity, the volume flow rate is not exactly proportional to the flow area occupied by the fluid. The interface position does equal the flow fraction at 0%, 50% and 100% of the channel width, but at all other locations the true flow fraction is farther from 50% than the interface location is. The correction factor can be found by using a finite difference model of laminar flow in a rectangular duct. The model solves a simplified Navier–Stokes equation,[49]

$$\frac{\partial^2 u}{\partial y^2} + \frac{\partial^2 u}{\partial z^2} + \mu \frac{\mathrm{d}p}{\mathrm{d}x} = 0 \qquad (2)$$

where u is the fluid velocity in the x direction, μ is the viscosity and $\mathrm{d}p/\mathrm{d}x$ is the pressure drop per unit length. The velocities are then integrated in the z direction and plotted as a function of y (Fig. S-1 in ESI†). A linear function can be fit to the central portion of the curve, which contains all of our flow fraction data (R^2 = 1.00; the fit region excludes 10% of the plot at each end). This function is applied to each measured boundary position to determine the actual flow fraction. A separate linear function is derived for each of the four channel widths used in the diluters.

The results of the ratiometric analysis are summarized in Fig. 8. Fig. 8A shows a plot of yellow and blue dye concentrations in the streams exiting the diluters, relative to those in the Y_3 and B_3 streams, respectively. As stated above, the ideal concentrations (free from fabrication or operation errors) of Y_1 and Y_2 are 33% and 67% of Y_3, respectively, and the ideal concentrations of B_1 and B_2 are 33% and 67% of B_3, respectively. The measured and ideal values differ by ~5% for Y_1, ~1% for Y_2, ~5% for the average of the four B_1 channels, and ~3% for the average of the four B_2 channels. Fig. 8B presents the measured fraction of yellow streams occupying each of the 16 channels in the joining array (top half of Fig. 2F). The average deviation from the ideal 50% ratio is 3.2% of the total channel width, demonstrating the ability of the network to distribute flows evenly among the outlet channels.

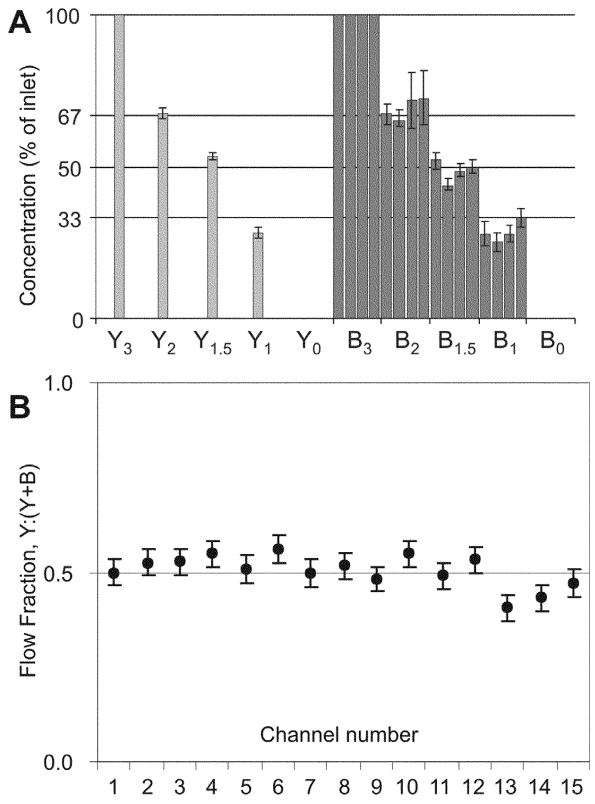

Fig. 8 Results of the ratiometric analysis. (A) Dye concentrations in the Y_3, Y_2, $Y_{1.5}$, and Y_1 streams (light gray bars, height depicting concentration relative to the Y_3 stream) and in the B_3, B_2, $B_{1.5}$, and B_1 streams (dark gray bars, height depicting concentration relative to the B_3 stream). Note that our device includes one yellow diluter and four blue diluters, together resulting in 5 and 20 data points, respectively. (B) Yellow flow fraction for each of the 16 outlet channels in the joining array (*e.g.*, Fig. 2F). A flow fraction of 0 corresponds to the yellow stream being absent from the outlet channel, and a flow fraction of 1 corresponds to the yellow stream occupying the entire outlet channel. Thus, the portion below each point is the fraction occupied by the yellow stream, and the remainder is occupied by blue stream. Note that channel 16 contained two clear streams so the interface position was not measurable. Error bars account for the accumulated uncertainty of two pixels' error on each distance measurement.

Upscaling complexity

The throughput benefits of a microfluidic combinatorial mixer grow with the number of unique mixtures that it creates. The number of dilutions of each compound can be increased by using higher-order diluters and distributors (*e.g.*, by adding stages to each module). If the distributors are composed of 2× distributors and each diluter uses the mixing network shown above, the flow balance is maintained by symmetry and a new analysis is not needed. Diluting into numbers other than powers of two would require distributors that are not inherently balanced, which may require further fluid dynamics analysis.

It is straightforward to generalize our current device and derive design rules for devices with more inlet compounds. Our device creates four dilutions of two compounds by using two fluidic networks (one for yellow dye and one for blue dye). Each network has two modules: one 2-stage diluter followed by two 2× distributors. Neither of the distributors for the yellow dye has bridges whereas both distributors for the blue dye have bridges. In general, combinatorial mixing with N input compounds and M dilutions per compound can be achieved by N networks (one for each compound), each of which has N modules. One of the N modules must be an $(M - 2)$-stage diluter (which outputs M dilutions) and the other $(N - 1)$ modules must be $M\times$ distributors, so the final sequence contains M^N channels. If M is different for each compound, the rules of combination must be modified slightly; for example, the power term M^N becomes a series product $(M_1 \cdot M_2 \cdot \ldots \cdot M_N)$. For any given network, the distributors placed upstream of the diluter must contain bridges and the distributors placed downstream of the diluter must not. It is convenient that M be a power of two ($M = 2^p$), so that an $M\times$ distributor can be formed by cascading p symmetric 2× distributors. This strategy confers equal flow resistance on all the flow paths, so it was used in every 4× distributor in our device.

Downscaling size

We chose several design options that are convenient for prototyping but could be changed if a smaller device footprint or smaller total fluid volume were required. For example, our device has been spread out to improve visualization. When visualization is not a concern, the networks for every compound can be condensed in a single stack. The size of the combinatorial device may also be reduced by using higher-resolution microfabrication techniques. The main advantage of cutting microchannels with a laser plotter is speed: the design can be fed into the laser cutter digitally, resulting in a patterned laminate in a few minutes. One option that retains the speed of laser cutting (albeit at higher cost) is to cut with a shorter-wavelength laser (*e.g.*, excimer laser). A more time-consuming but precise alternative to laser cutting is to use soft lithography, based on molding poly-dimethylsiloxane (PDMS) from a photolithographic master.[50,51] Soft lithography provides better lateral resolution and avoids the problem mentioned earlier of bead formation around windows. Although the flexible elastomeric laminates are not as easily aligned, complex 3D microfluidic devices have been demonstrated.[52–54] In addition, the use of two-level photolithography enables a single layer of PDMS to include a flow level plus its corresponding window layer.[38] Therefore, the number of alignment steps for a PDMS device can be half of the number needed for a geometrically similar Mylar device. In fact, the entire

device could be constructed with only two flow levels (plus corresponding windows), by using one level for bridges and one level for all other features; this design would reduce the number of alignment steps at the expense of increasing the total area.

Conclusions

Our microfluidic combinatorial mixer continuously produces 16 chemically unique outputs from two dye solutions and two diluent inputs, for a time span that is limited only by its external pumping source. The fluidic network is balanced by symmetry, subject to the precision of the cutting method, assembly process, and pumping rates. Analysis of the laminar flow patterns shows that the concentration levels are close to the desired linear progression when flows are equal at all inlets. Serpentine mixers with as few as two coils perform well at low flow rates with absorbent dyes (mol. wt. = 500–800). Short mixers would be appropriate for constant-flow applications that require low fluid shear (*e.g.*, a cell-containing bioreactor), while coils can be added easily to designs for applications requiring high flow rates (*e.g.*, high throughput testing or higher molecular weight compounds).

Combinatorial mixers can be paired with cell patterning techniques and biosensors to increase the complexity and throughput of biochemical analyses. For example, a mixer could be used to pattern combinations of adhesion proteins and/or expose cells to combinations of growth and signaling factors, nutrients, or drugs to test their combined influence on cell adhesion and growth. Running simultaneous experiments in a minimal area would reduce the required resources while increasing the number of cells and fluidic environments under microscopic observation. More generally, the combinatorial mixer has the potential to multiply the number of experimental samples that can be tested without increasing demands on time, material and/or equipment resources.

Acknowledgements

This work was supported by Micronics, Inc., and the Washington Technology Center at the University of Washington. We also thank Bernhard Weigl (Micronics), Andrew Kamholz, Matt Munson and Catherine Cabrera (all UW Department of Bioengineering) for their valuable insight on micromixers and Mylar device assembly. We are indebted to Paul Yager (UW Department of Bioengineering) for lending pumping equipment.

References and notes

1 D. L. Nelson and M. M. Cox, *Lehninger Principles of Biochemistry*, Worth Publishers, New York, 2000.
2 R. I. Freshney, *Culture of Animal Cells: A Manual of Basic Techniques*, Wiley-Liss, New York, 4th edn., 2000.
3 D. J. Harrison, A. Manz, Z. H. Fan, H. Ludi and H. M. Widmer, *Anal. Chem.*, 1992, **64**, 1926–1932.
4 A. Manz, D. J. Harrison, E. M. J. Verpoorte, J. C. Fettinger, A. Paulus, H. Ludi and H. M. Widmer, *J. Chromatogr., A*, 1992, **593**, 253–258.
5 V. Dolnik, S. R. Liu and S. Jovanovich, *Electrophoresis*, 2000, **21**, 41–54.
6 O. Niwa, *Electroanalysis*, 1995, **7**, 606–613.
7 P. G. Vahey, S. H. Park, B. J. Marquardt, Y. N. Xia, L. W. Burgess and R. E. Synovec, *Talanta*, 2000, **51**, 1205–1212.
8 J. C. T. Eijkel, H. Stoeri and A. Manz, *Anal. Chem.*, 2000, **72**, 2547–2552.
9 A. T. Woolley and R. A. Mathies, *Anal. Chem.*, 1995, **67**, 3676–3680.
10 S. Ekstrom, P. Onnerfjord, J. Nilsson, M. Bengtsson, T. Laurell and G. Marko-Varga, *Anal. Chem.*, 2000, **72**, 286–293.
11 J. J. Li, J. F. Kelly, I. Chemushevich, D. J. Harrison and P. Thibault, *Anal. Chem.*, 2000, **72**, 599–609.
12 O. Niwa, R. Kurita, Z. M. Liu, T. Horiuchi and K. Torimitsue, *Anal. Chem.*, 2000, **72**, 949–955.
13 B. L. Zhang, F. Foret and B. L. Karger, *Anal. Chem.*, 2000, **72**, 1015–1022.
14 I. Karube and K. Yokoyama, *Sens. Actuators, Part B*, 1993, **13**, 12–15.
15 J. Wang, M. P. Chatrathi, B. M. Tian and R. Polsky, *Anal. Chem.*, 2000, **72**, 2514–2518.
16 A. Y. Fu, C. Spence, A. Scherer, F. H. Arnold and S. R. Quake, *Nat. Biotechnol.*, 1999, **17**, 1109–1111.
17 J. Oakey, J. Allely and D. W. M. Marr, *Biotechnol. Prog.*, 2002, **18**, 1439–1442.
18 P. C. Li and D. J. Harrison, *Anal. Chem.*, 1997, **69**, 1564–1568.
19 J. Chen, K. D. Wise, J. F. Hetke and S. C. Bledsoe, Jr, *IEEE Trans. Biomed. Eng.*, 1997, **44**, 760–769.
20 A. Sanjoh and T. Tsukihara, *J. Cryst. Growth*, 1999, **196**, 691–702.
21 C. L. Hansen, E. Skordalakes, J. M. Berger and S. R. Quake, *PNAS*, 2002, **99**, 16531–16536.
22 A. Hatch, A. E. Kamholz, K. R. Hawkins, M. S. Munson, E. A. Schilling, B. H. Weigl and P. Yager, *Nat. Biotechnol.*, 2001, **19**, 461–465.
23 E. M. Purcell, *Am. J. Phys.*, 1977, **45**, 3–11.
24 G. E. Karniadakis and A. Beskok, *Micro Flows*, Springer-Verlag, New York, 2002.
25 N. Harnby, M. Edwards and A. Nienow, *Mixing in the Process Industries* , Butterworth, Oxford, 1992.
26 N. Schwesinger, H. Frank and H. Wurmus, *J. Micromech. Microeng.*, 1996, **6**, 99–102.
27 J. Branebjerg, P. Gravesen, J. P. Krog and C. R. Nielsen, *MEMS 96: Proc. 9th Ann. Int. Work. Micro Electro Mech. Syst. San Diego, CA, USA, 11–15 February 1996*; IEEE; 441–446.
28 F. G. Bessoth, A. J. deMello and A. Manz, *Anal. Commun.*, 1999, **36**, 213–215.
29 S. W. Jones, O. M. Thomas and H. Aref, *J. Fluid Mech.*, 1989, **209**, 335–357.
30 R. H. Liu, M. A. Stremler, K. V. Sharp, M. G. Olsen, J. G. Santiago, R. J. Adrian, H. Aref and D. J. Beebe, *J. Microelectromech. Syst.*, 2000, **9**, 190–197.
31 D. Therriault, S. R. White and J. A. Lewis, *Nat. Mater.*, 2003, **2**, 265–271.
32 A. D. Stroock, S. K. W. Dertinger, A. Ajdari, I. Mezic, H. A. Stone and G. M. Whitesides, *Science*, 2002, **295**, 647–651.
33 M. Elwenspoek, T. S. J. Lammerink, R. Miyake and J. H. J. Fluitman, *J. Micromech. Microeng.*, 1994, **4**, 227–45.
34 S. C. Jacobson, T. E. McKnight and J. M. Ramsey, *Anal. Chem.*, 1999, **71**, 4455–4459.
35 J. P. Kutter, S. C. Jacobson and J. M. Ramsey, *Anal. Chem.*, 1997, **69**, 5165–5171.
36 S. K. W. Dertinger, D. T. Chiu, N. L. Jeon and G. M. Whitesides, *Anal. Chem.*, 2001, **73**, 1240–1246.
37 B. H. Jo, L. M. Van Lerberghe, K. M. Motsegood and D. J. Beebe, *J. Microelectromech. Syst.*, 2000, **9**, 76–81.
38 J. R. Anderson, D. T. Chiu, R. J. Jackman, O. Cherniavskaya, J. C. McDonald, H. K. Wu, S. H. Whitesides and G. M. Whitesides, *Anal. Chem.*, 2000, **72**, 3158–3164.
39 R. F. Ismagilov, D. Rosmarin, P. J. A. Kenis, D. T. Chiu, W. Zhang, H. A. Stone and G. M. Whitesides, *Anal. Chem.*, 2001, **73**, 4682–4687.
40 R. F. Ismagilov, J. M. K. Ng, P. J. A. Kenis and G. M. Whitesides, *Anal. Chem.*, 2001, **73**, 5207–5213.
41 P. C. Wang, D. L. DeVoe and C. S. Lee, *Electrophoresis*, 2001, **22**, 3857–3867.
42 Y. Kikutani, H. Hisamoto, M. Tokeshi and T. Kitamori, in *Micro Total Analysis Systems 2001*, ed. J. M. Ramsey and A. van den Berg, Kluwer Academic, Boston, 2001, pp. 161–162.
43 H.-P. Chou, M. A. Unger and S. R. Quake, *Biomed. Microdev.*, 2001, **3**, 323–330.
44 J. Liu, M. Enzelberger and S. Quake, *Electrophoresis*, 2002, **23**, 1531–1536.
45 The diffusion coefficient of the dyes was extrapolated from published values for smaller compounds (100–200 Da), assuming that the coefficient was inversely proportional to the cube root of the molecular weight of the solute (Tanford, C., *Physical Chemistry of Macromolecules*, 1961, John Wiley & Sons, New York). The formula weights of Yellow #6 and Blue #1 are 452 Da and 793 Da, respectively.
46 Although light transmittance is a non-linear indicator of dye concentration, it is an excellent indicator of the uniformity of the concentration field. Admittedly, the photographs show only horizontal concentration gradients and do not reveal vertical gradients. It is possible for a serpentine channel to redistribute two incoming streams in a manner that maintains vertical gradients while appearing uniform from the top (uniform flow layering). However, Fig. 5 and Fig. 6 indicate that the flow layering in our flat serpentine mixers is not uniform. The twists leave an unlayered region along the lateral edge of each channel, where we have observed the highest (or lowest) concentration to be. Therefore, we consider that a uniform dye appearance does indicate sufficient

mixing for our application. More accurate measures of mixing can be made by confocal micrsocopy (*e.g.*, ref 32) or fluorescence techniques (*e.g.*, M. S. Munson and P. Yager, *Anal. Chim. Acta*, 2004, **507**, 63–71.
47 H. S. Fogler, *Elements of Chemical Reaction Engineering*, Prentice-Hall, Englewood Cliffs, NJ, 3rd edn., 1999.
48 P. M. B. Walker, *Dictionary of Science and Technology*, Chambers Harrap, Edinburgh, 1999.
49 K. A. Hoffmann and S. T. Chiang, *Computational Fluid Dynamics for Engineers*, Engineering Education System, Wichita, KS, 1993.
50 Y. N. Xia and G. M. Whitesides, *Angew. Chem. Int. Ed. Engl.*, 1998, **37**, 551.
51 D. C. Duffy, J. C. McDonald, O. J. A. Schueller and G. M. Whitesides, *Anal. Chem.*, 1998, **70**, 4974–4984.
52 D. T. Chiu, E. Pezzoli, H. K. Wu, A. D. Stroock and G. M. Whitesides, *Proc. Natl. Acad. Sci. USA*, 2001, **98**, 2961–2966.
53 M. A. Unger, H. P. Chou, T. Thorsen, A. Scherer and S. R. Quake, *Science*, 2000, **288**, 113–116.
54 T. Thorsen, S. J. Maerkl and S. R. Quake, *Science*, 2002, **298**, 580–584.